Supporting Information for

Nacre-mimetic Calcium Silicate Hydrate (C-S-H) Composite with High Strength and Toughness

Chenchen Xiong [a,b], Weihuan Li [a,b], Jiarui Xing [a,b], Shengjun Chen [a,b], Yulin Wang [a,b], Yang Zhou [a, b, *]

a School of Materials Science and Engineering, Southeast University, Nanjing 211189, China

b State Key Laboratory of Engineering Materials for Major Infrastructure, Southeast University, Nanjing 211189, China

Supplementary methods

Molecular dynamics simulation

Following the process in Ref. [1], C-S-H models employed was built according to the "realistic model" proposed by Pellenq et al. [2], which has been widely applied into the simulation of cement-based materials. First, the C-S-H model with Ca/Si of 1.3 was cleaved along with the [0 0 1] direction to create the C-S-H interface for polymer molecule absorption on the interlayer space, which was a widely used method for simulating the organic-inorganic interaction in C-S-H systems [3]. Then, layered C-S-H models were built by the ordered arrangement of unit cell and several water molecules were filled into the space between C-S-H matrix to imitate the gel pore. Based on the experimentally observed layered structure, C-S-H and epoxy resin alternating structure were constructed to investigate the influence of varying polymer contents and layer thickness ratio on structural properties, mechanical performance, and fracture behavior, aiming to enhance the understanding of strengthening and toughening mechanisms. In

* Corresponding author at: School of Materials Science and Engineering, Southeast University, Nanjing 211189, China. E-mail: tomaszy@seu.edu.cn

detail, epoxy chains were inserted between the established C-S-H layers along z-direction, where models with 1-layer, 2-layer and 3-layer polymer, corresponding to 3-thickness C-S-H, 2-thickness and 1-thickness C-S-H, were named CSH-L1, CSH-L2, and CSH-L3 (Figure S9). The calculation process is as follows. Initially, the system was equilibrated in the NPT ensemble at 300 K and 1 atm for 300 ps, with a step size of 0.5 fs. Subsequently, the uniaxial tensile simulation along X-direction was carried out, with a strain rate of 0.005 ps^{-1} and a simulation time of 240 ps. The stress and strain along the deformation direction were recorded for statistical analysis.

Density functional theory (DFT) calculation

The employed model was constructed by placing an epoxy resin model on 14 Å tobermorite (Figure S9), referred to the previous studies [4]. Calculations were performed using CP2K software with the Quickstep code [5, 6], which provides framework for DFT methods using the mixed Gaussian and plane waves approaches (GPW). The generalized gradient approximation with Perdew Burke Ernzerhof (GGA-PBE) [7] exchange-correlation functional was used with the Grimme D3 correction [8]. The Goedecker-Teter-Hutter (GTH) [9, 10] pseudopotentials were employed to described the core electrons when the double-zeta valence polarized (DZVP) basis set with an energy-cutoff of 600 Ry was used to depicted the valence electrons. The orbital transformation (OT) method was used while the convergence criterion energy was set to 10^{-12} Hartree and the target accuracy for the self-consistent field (SCF) convergence was set to 10^{-7} Hartree.

Finite element method (FEM) simulation

In the simulation, due to the limitation of ABAQUS unit division and computational power, the structural thickness of each layer has to be increased compared to experimental results, and a 3D BM structure (20mm×2mm×4mm) was adopted as shown in Figure S11, containing staggered arrangement of bricks bonded by the thin layer of mortar, which was modeled as a cohesive zone. The thickness and length of C-

S-H brick is set 0.2 mm and 2 mm, respectively. Based on the intrinsic properties of C-S-H and cement-based "brick-mortar" model from Ref. [3, 11], the C-S-H bricks with an isotropic bulk modulus of 20 GPa, a Poisson's ratio of 0.2 and a density of 2.39 g/cm^3 bear elastic deformation before failure. A traction-separation law was selected to describe the interfacial behavior of the cohesive elements [12]. The rigid cylinders of the bottom support were fixed with a span of 12 mm and the loading was applied through the rigid cylinder at the top center.

Supplementary experimental data and analysis

Figure S1. Stability of C-S-H suspension with (right) and without (left) PVA manipulation indicating the inhibited agglomeration of C-S-H

Supplementary note 1

The morphology of long-range oriented C-S-H structures under various polymer content and C-S-H concentrations exhibited distinct characteristics as shown in Figure S2, S3. Specifically, low polymer concentration resulted in reduced viscosity, which excessively accelerated ice crystal growth, thereby diminishing the effectiveness of the dual temperature gradient and consequently leading to insufficient alignment of the ice crystals. As the polymer concentration increased, the formation of interlayer bridges was observed with retained considerable pores and limited orientation. With the polymer concentration increased to 10 wt%, the temperature gradient drove stable ice crystal aligned growth under the marked increased viscosity, facilitating the ordered arrangement of C-S-H particles and yielding a highly oriented layered structure. It should be noted that excessively increased viscosity inhibited ice crystal growth, which

led to C-S-H struggled to separate to form oriented arrangement, characterized by the microstructure without connected pores and hierarchical structure.

While the optimal polymer concentration in the preparation of C-S-H scaffolds under stably ordered growth was obtained (Figure S2), the C-S-H content also significantly influenced the microstructure. With the increase of C-S-H concentration, the layer thickness increased in C-S-H scaffold and C-S-H aggregates may appear (Figure S3). Through the manipulation of the organic/inorganic ratio, we can achieve C-S-H scaffolds with different layer thickness, where the long-range ordered structure played a crucial role in the nacre-mimetic architecture. Bridges, waves and protrusions formed by densified procedure mimicked the energy dissipation and toughening mechanisms in natural nacre as shown in Figure S3.

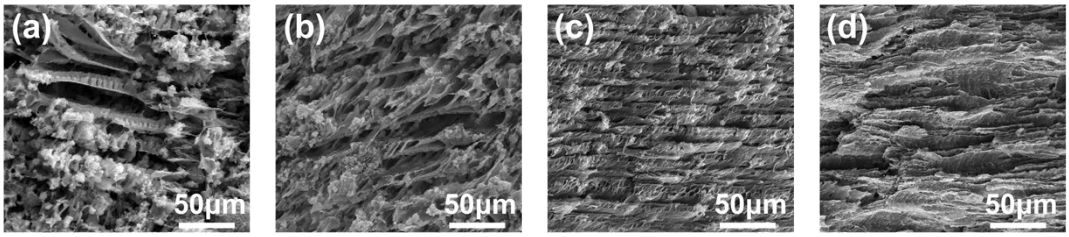

Figure S2. Different oriented C-S-H scaffolds with various PVA contents of (a) 5%, (b) 7%, (c) 10%, (d)13%

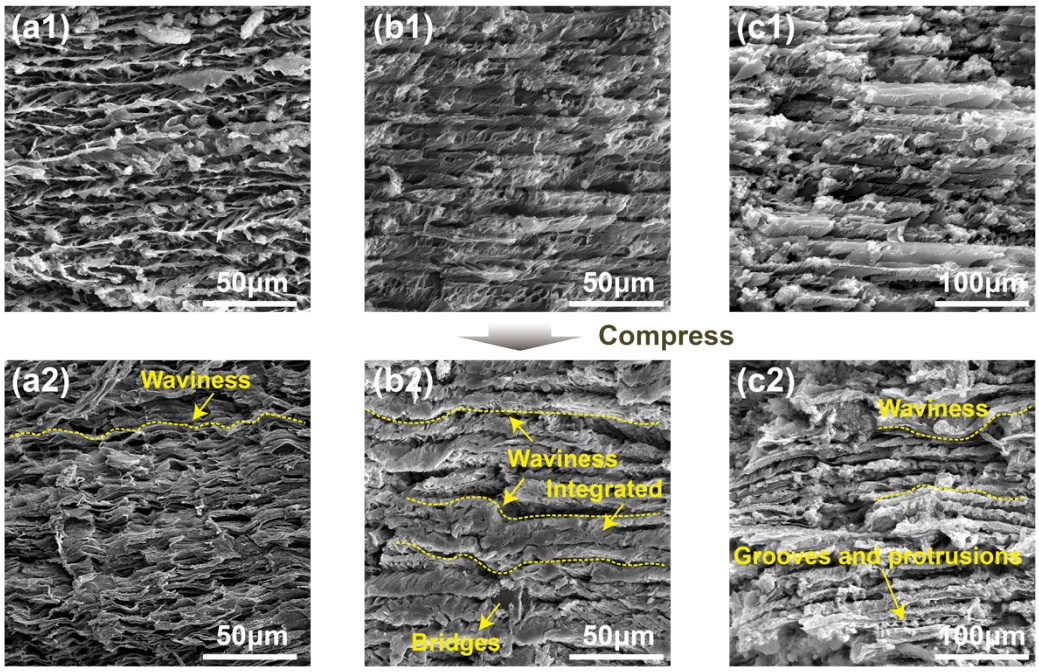

Figure S3. Morphologies of C-S-H scaffolds and densified C-S-H scaffolds with various C-S-H concentrations (a) 0.5 M, (b) 0.75 M, (c) 1.0 M

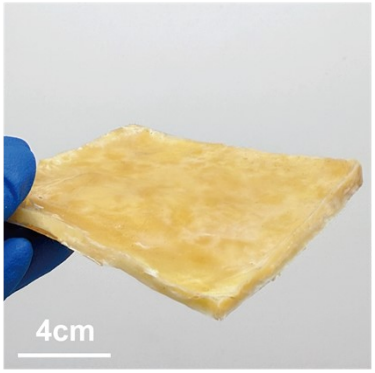

Figure S4. Digital photograph of macro-characterization of large-sized nacre-mimetic C-S-H composite

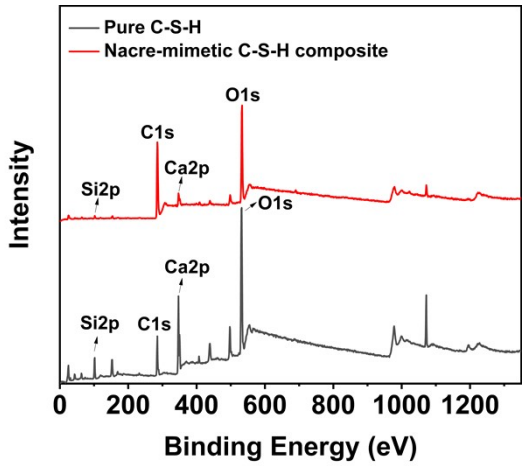

Figure S5. XPS spectrum of pure C-S-H and nacre-mimetic C-S-H samples

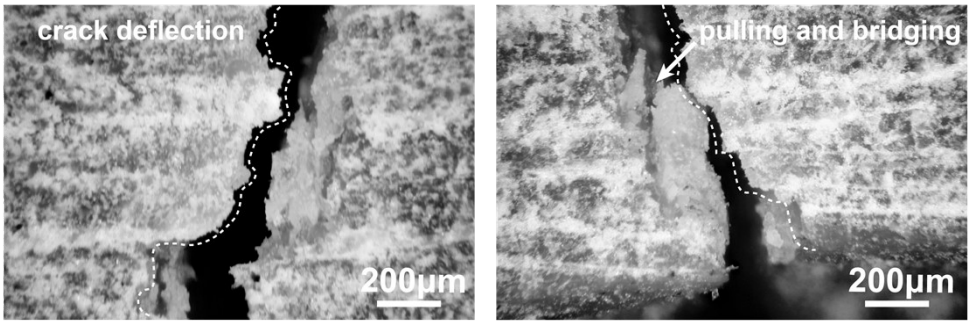

Figure S6. Crack deflection with pulling and bridging effects occurred in nacre-mimetic C-S-H composite under flexural tests

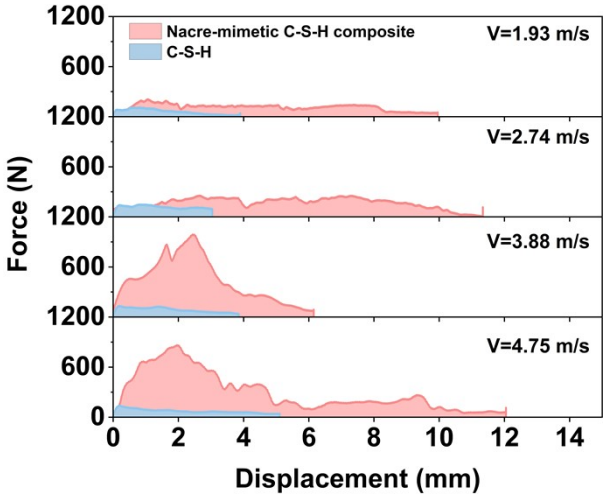

Figure S7. Force-displacement curves of pure C-S-H and nacre-mimetic C-S-H composite under different impact velocity

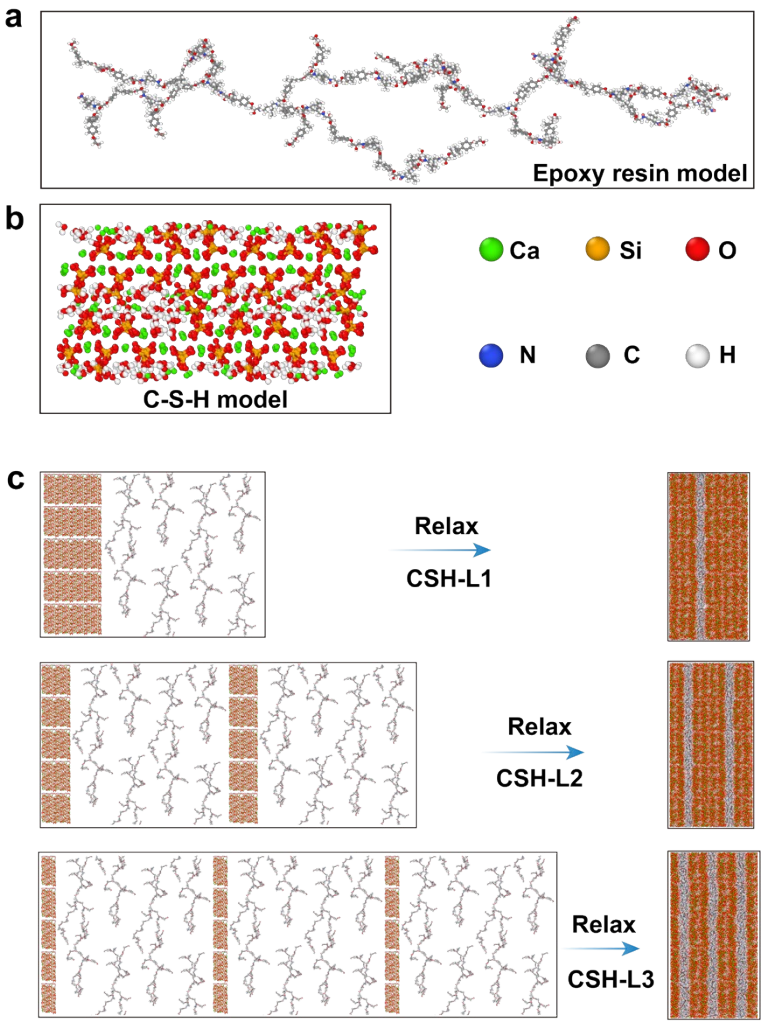

Figure S8. Initial models of MD simulations

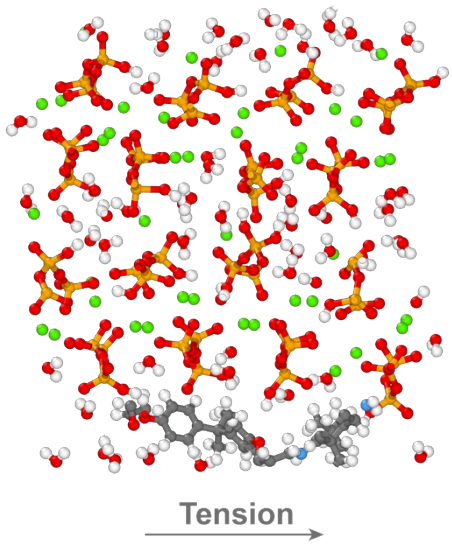

Figure S9. Initial model of DFT calculations

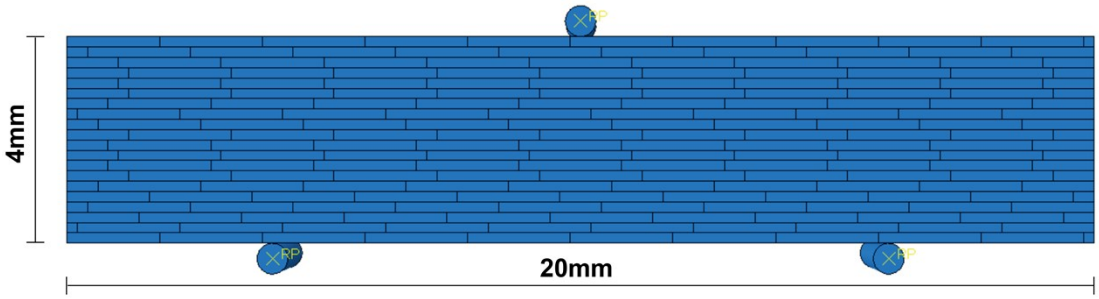

Figure S10. Initial model of FEM simulations

Table S1. Data origin of Ashby plot of flexural strength, ultimate strain and toughness (Some of the data are roughly estimated by the stress-strain curve provided)

Natural materials / Artificial composites		Organic content (%)	Flexural strength (MPa)	Flexural strain (%)	Toughness (MJ/m^3)	References
Natural materials	AW nacre	~5	124.2±10.3	0.32	0.192	[13]
	Nacre	~5	98.097	0.56	0.402	[14]
	AV nacre	~5	70	0.70	0.245	[15]
	C. plicata shell	~5	90-180	0.18-3.5	0.081-2.925	[16]
	Aragonite	-	57.2	0.13	0.037	[13]
	Wood	-	54.3	~10	3.3941	[17]
Fiber/polymer/nanomaterials reinforced cementitious composites	Cement	-	5.5-11	0.077-0.22	0.0017-0.0097	[18-21]
	Cement/PVA/CNT	0.1	8-10	-	-	[22]
	Cement/SBR	1-20	5-9	-	-	[18]
	Cement/Epoxy resin	10-20	2.1-2.8	-	-	[23]
	Cement/Rubber	2.5-10	2.3-2.4	-	-	[23]
	Cement/PAM	0.3-5	13.5-25.7	-	-	[24]

	Cement/UHMWPE	15-50	6.1-18.2	2.5-9.5	0.0223-1.3916	[19]
	Cement/UHMWPE/fiber	~20	28.1	~2	0.5850	[19]
	Cement/copolyester fiber	0.1	5.7	~2	0.0305	[19]
	Cement/PVA/SBR	0.1-0.4	3.8-4.8	-	-	[20]
	Cement/steel fiber	8-12	15.93-44.02	-	-	[25]
	Cement/PP fiber	8-12	11.13-15.73	-	-	[25]
	Cement/steel fiber/PP fiber	8-12	10.11-41.23	-	-	[25]
	Cement/steel fiber	0.5-2.5	3.42-7.09	1.0-1.67	0.019-0.063	[26]
	Cement/steel fiber	0.2-1.0	4.53-8.31	0.4-1.0	0.004-0.046	[27]
	Cement/ cellulosic fiber	4-16	8-12	0.7-4.6	0.0278-0.2693	[21]
	Cement/CNT	0.1-0.3	8.17-11.26	~1.2	0.0376-0.0881	[28]
	Cement/graphite	0.1-0.3	8.49-12.31	~1.2	0.050-0.133	[28]
Nacre-inspired cementitious composites	Cement/ABS	-	12-24	0.38-2.27	0.025-0.4	[29]
	“Brick-mortar” cement	~1	~0.5	~30	0.065	[30]
	Cement/steel/polymeric layers	-	58.3	~1	0.2457	[31]
	Cement/PAM/EVA	-	14-18	1-3	0.06-0.16	[12]
	Cement/PVC	2.55-3.14	12-17	5-12	0.5-1.5	[32]

	Cement/PVA	-	3-7	1-35	0.04-1.47	[3]
	Cement/Resin	-	25-66	0.7-4	0.027-0.854	[33]
	Cement/PVA/gelatin	12-22	12-45	7-18	0.595-2.025	[34]
C-S-H-based composites	C-S-H	-	2-6	~3.3	~0.081	[35]
	C-S-H/SBR	5-15	9.69-12.3	0.2-0.8	0.013-0.049	[36]
	C-S-H/SA	6.5-11.4	34.3-41.2	0.20-0.28	0.034-0.056	[37]
	C-S-H/GO	0.66-1.96	5-26.39	-	0.0272-0.1222	[11]
	Hot-pressing C-S-H/polymers	30~70	22-124	1.36-14.93	0.1586-5.1725	[38]
This work	Nacre C-S-H	43.8-65.3	42.72-68.90	20.80-32.23	6.85-7.79	Our work

Table S2. Impact resistance comparison between the nacre-mimetic C-S-H composite and representative natural/artificial materials

Materials	**Impact energy/ J**	**Impact velocity/ $m \cdot s^{-1}$**	**Density/ $g \cdot cm^{-3}$**	**Peak force/ N**	**Energy absorption/ J**	**Specific peak force/N g^{-1} cm^3**	**Specific energy adsorption/J g^{-1} cm^3**	**Reference**
Alumina	1	0.934	≈3.99	415.39-486.81	0.0455-0.0511	104.10-122.01	0.0114-0.0128	[39]
Nacre-like ceramic composites	1	0.934	≈2.8	466.38-674.04	0.0694-0.0796	166.56-240.73	0.0248-0.0284	[39]
Nacre-like ceramic composites	1	0.934	≈2.8	544.68-755.75	0.0547-0.0865	194.53-269.91	0.0195-0.0309	[39]
Solid ceramic	30	3.65	2.4-2.9	298.70-566.65	0.04-0.70	103-236.10	0.01379-0.2917	[40]
Orthogonal polycarbonate	30	3.65	≈1.55	468.66-717.17	2.70-5.55	302.36-462.69	1.7419-3.5806	[40]

Gradient Bouligand polymethyl methacrylate	30	3.65	≈1.55	1020.22-1323.12	3.04-4.40	658.21-853.63	1.9613-2.8387	[40]
Gradient Bouligand thermoplastic poly-urethanes	30	3.65	≈1.55	557.18-650.37	4.98-9.68	359.47-419.59	3.2129-6.2452	[40]
Gradient Bouligand polycarbonate	30	3.65	≈1.55	1116.37-1597.88	4.55-11.26	720.24-1030.89	2.9355-7.2645	[40]
Bouligand polycarbonate	30	3.65	≈1.55	805.76-1143.61	5.25-9.10	519.84-737.81	3.3871-5.8710	[40]
Gradient cement composites	18	3.84	≈2.1	20315.6 ~22951.8	10.982~ 17.835	9674.10-10929.43	5.2295-8.4928	[33]
Heterogeneous cement composites	8	2.56	≈2.1	14728.2	7.353	7013.43	3.5014	[33]
Nacre-like glass composite	0.375-13.5	1.0-6.0	2.23	150-200	0.3-2	67.26-89.59	0.1345-0.8969	[41]
Laminated glass composite	0.375-13.5	1.0-6.0	2.23	750-1000	0.1-2.5	336.32-448.43	0.0448-1.1211	[41]
Glass	0.375-13.5	1.0-6.0	2.23	1000-1500	0.1-1.7	448.43-672.64	0.0448-0.7623	[41]
Cement	1.181	0.99	≈2	293.23	0.030	146.615	0.015	[33]
Bouligand wood	2.05	2.34	1.4	1570.7	≈1.9	1121.928571	1.357142857	[42]
Nacre-like polyborosiloxane composites	0.175-0.7	1.0-2.0	0.65	60-285	0.1-0.6	92.31-438.46	0.1538-0.9231	[43]
Nacre-like ceramic composite	4.5	1.36	3.875	300-1000	1.0-2.0	77.42-258.06	0.2581-0.5161	[44]
Nacre-like glass composite	1.3689	2.34	≈1.8	-	0.5-1.6	-	0.2778-0.8889	[45]
Prestress nacre-inspired polymer	6.67	2.48	3	700-1400	6-7.5	233.33-466.67	2-2.5	[46]

composite								
Traditional C-S-H	5-30	1.93-4.75	≈2.39	111.16-149.21	0.23-0.37	46.51-62.43	0.0954-0.1542	Our work
Nacre C-S-H	5-30	1.93-4.75	≈0.95	209.60-988.55	1.12-3.56	220.63-1040.58	1.1809-3.7468	Our work

Table S3. Potential parameters of ClayFF

Species	Charge (e)	D_0 (kcal/mol)	R_0 (Å)
Hydroxide calcium	1.050	$5.0298*10^{-6}$	6.2428
Aqueous calcium ion	2.000	0.1	3.2237
Tetrahedral silicon	2.100	$1.8405*10^{-6}$	3.7064
Bridge oxygen	-1.050	0.1554	3.5532
Hydroxyl oxygen	-0.950	0.1554	3.5532
Water oxygen	-0.820	0.1554	3.5532
Water hydrogen	0.410	-	-
Hydroxyl hydrogen	0.425	-	-

Table S4. Potential parameters of CVFF

Species	Charge (e)	D_0 (kJ/mol)	R_0 (Å)
Methyl carbon	-0.300	0.163	3.8754
sp^3 carbon bonded to 2H atoms	-0.200	0.163	3.8754
sp^3 carbon bonded to 1H atom	0.578	0.163	3.8754
Hydrogen bonded to C	0.100	0.159	2.4500
Hydrogen bonded to O	0.350	0.000	0.0000
Nitrogen	-0.580	0.6987	3.5012

Table S5. Energy absorption under tension

Samples	Energy absorption (MJ)
CSH	155.50
CSH-L1	195.67
CSH-L2	227.88

CSH-L3	227.95

References

1. W. Li, C. Xiong, Y. Zhou, W. Chen, Y. Zheng, W. Lin and J. Xing, Cem. Concr. Res., 2024, 186.
2. R. J. M. Pellenq, A. Kushima, R. Shahsavari, K. J. Van Vliet, M. J. Buehler, S. Yip and F. J. Ulm, Proc. Natl. Acad. Sci. U.S.A., 2009, 106, 16102-16107.
3. Y. Chen, Y. Zheng, Y. Zhou, W. Zhang, W. Li, W. She, J. Liu and C. Miao, Nat. Commun., 2023, 14, 3438.
4. Y. Zhou, H. Zheng, W. Li, T. Ma and C. Miao, Cem. Concr. Res., 2022, 152.
5. T. D. Kühne, M. Iannuzzi, M. Del Ben, V. V. Rybkin, P. Seewald, F. Stein, T. Laino, R. Z. Khaliullin, O. Schütt, F. Schiffmann, D. Golze, J. Wilhelm, S. Chulkov, M. H. Bani-Hashemian, V. Weber, U. Borstnik, M. Taillefumier, A. S. Jakobovits, A. Lazzaro, H. Pabst, T. Müller, R. Schade, M. Guidon, S. Andermatt, N. Holmberg, G. K. Schenter, A. Hehn, A. Bussy, F. Belleflamme, G. Tabacchi, A. Glöss, M. Lass, I. Bethune, C. J. Mundy, C. Plessl, M. Watkins, J. VandeVondele, M. Krack and J. Hutter, J. Chem. Phys., 2020, 152.
6. J. VandeVondele, M. Krack, F. Mohamed, M. Parrinello, T. Chassaing and J. Hutter, Comput. Phys. Commun., 2005, 167, 103-128.
7. J. P. Perdew, K. Burke and M. Ernzerhof, Phys. Rev. Lett., 1996, 77, 3865-3868.
8. S. Grimme, J. Antony, S. Ehrlich and H. Krieg, J. Chem. Phys., 2010, 132.
9. C. Hartwigsen, S. Goedecker and J. Hutter, Phys. Rev. B, 1998, 58, 3641-3662.
10. S. Goedecker, M. Teter and J. Hutter, Phys. Rev. B, 1996, 54, 1703-1710.
11. K. Song, J. Liu, J. Dong, Y. Liang, T. Du, H. Fan and Q. Zhang, Carbon, 2025, 240.
12. H. Pan, W. She, W. Zuo, Y. Zhou, J. Huang, Z. Zhang, Z. Geng, Y. Yao, W. Zhang, L. Zheng, C. Miao and J. Liu, ACS Appl. Mater. Interfaces, 2020, 12, 53297-53309.
13. L. B. Mao, H. L. Gao, H. B. Yao, L. Liu, H. Cölfen, G. Liu, S. M. Chen, S. K. Li, Y. X. Yan, Y. Y. Liu and S. H. Yu, Science, 2016, 354, 107-110.
14. U. G. Wegst, H. Bai, E. Saiz, A. P. Tomsia and R. O. Ritchie, Nat. Mater., 2015, 14, 23-36.
15. Y. Chen, J. Fu, B. Dang, Q. Sun, H. Li and T. Zhai, ACS Nano, 2020, 14, 2036-2043.
16. S. M. Liang, H. M. Ji and X. W. Li, J. Mater. Sci. Technol., 2020, 44, 1-8.
17. J. Song, C. Chen, S. Zhu, M. Zhu, J. Dai, U. Ray, Y. Li, Y. Kuang, Y. Li, N. Quispe, Y. Yao, A. Gong, U. H. Leiste, H. A. Bruck, J. Y. Zhu, A. Vellore, H. Li, M. L. Minus, Z. Jia, A. Martini, T. Li and L. Hu, Nature, 2018, 554, 224-228.
18. R. Wang, P. M. Wang and X. G. Li, Cem. Concr. Res., 2005, 35, 900-906.
19. G. Sun, R. Liang, J. Zhang, Z. Li and L.-T. Weng, Cem. Concr. Compos., 2017, 78, 57-62.
20. J. J. Assaad, Constr. Build. Mater., 2018, 163, 139-148.
21. X. Xie, Z. Zhou and Y. Yan, Constr. Build. Mater., 2019, 220, 403-414.
22. Y. Zhao, J. Zhang, G. Qiao, D. Hou, B. Dong and H. Ma, ACS Appl. Nano Mater., 2022, 5, 6877-6889.
23. M. A. Fernández-Ruiz, L. M. Gil-Martín, J. F. Carbonell-Márquez and E. Hernández-Montes, Constr. Build. Mater., 2018, 173, 49-57.
24. R. Liang, Q. Liu, D. Hou, Z. Li and G. Sun, Cem. Concr. Res., 2022, 152.
25. M. Ipek and M. Aksu, Constr. Build. Mater., 2019, 214, 207-218.
26. J. j. Li, C. j. Wan, J. g. Niu, L. f. Wu and Y. c. Wu, Constr. Build. Mater., 2017, 131, 449-458.
27. J.-P. Won, B.-T. Hong, T.-J. Choi, S.-J. Lee and J.-W. Kang, Compos. Struct., 2012, 94, 1443-1449.

28. W. Meng and K. H. Khayat, Compos B Eng, 2016, 107, 113-122.
29. J. A. Rosewitz, H. A. Choshali and N. Rahbar, Cem. Concr. Compos., 2019, 96, 252-265.
30. V. Restrepo and R. V. Martinez, Mater. Des., 2021, 205.
31. Y. Mei, J. Liu, Y. Cui, F. Li, X. Tang, M. Sun, R. Chi, Y. Zhang, A. Zhang and K. Chen, Sci. Rep., 2021, 11.
32. J. Ye, K. Yu, J. Yu, Q. Zhang and L. Li, Cem. Concr. Compos., 2021, 118.
33. Z. Y. Wu, H. Pan, P. Huang, J. H. Tang and W. She, Adv. Mater., 2024, 36.
34. J. Chen, Z. Liu, S. Zhang, S. Hu and F. Wang, Adv Sci (Weinh), 2025, 12, e03854.
35. Y. H. Wang, S. Goodman, Y. Bao and W. A. Meng, Cement Concrete Comp, 2023, 143.
36. J. Starr, E. M. Soliman, E. N. Matteo, T. Dewers, J. C. Stormont and M. M. Reda Taha, Cem. Concr. Compos., 2021, 124.
37. C. Gao, H. Zeng, J. Xu, D. Xu, Y. Ma, W. She, Z. Hu, J. Tang and J. Liu, Cem. Concr. Res., 2025, 187.
38. Y. Wang, Y. Bao and W. Meng, ACS Nano, 2024, 18, 23655-23671.
39. Z. B. Zhang, H. L. Gao, S. M. Wen, J. Pang, S. C. Zhang, C. Cui, Z. Y. Wang and S. H. Yu, Adv. Mater., 2023, 35.
40. S. M. Wen, S. M. Chen, W. Gao, Z. Zheng, J. Z. Bao, C. Cui, S. Liu, H. L. Gao and S. H. Yu, Adv. Mater., 2023, 35.
41. X. Zhang, K. Wu, Y. Ni and L. He, Nat. Commun., 2022, 13.
42. Y. Chen, B. Dang, J. Fu, J. Zhang, H. Liang, Q. Sun, T. Zhai and H. Li, ACS Nano, 2022, 16, 7525-7534.
43. S. Liu, S. Wang, M. Sang, J. Zhou, J. Zhang, S. Xuan and X. Gong, ACS Nano, 2022, 16, 19067-19086.
44. H. Yazdani Sarvestani, D. Aranguren van Egmond, I. Esmail, M. Genest, C. Paquet and B. Ashrafi, Adv. Funct. Mater., 2021, 32.
45. Z. Yin, F. Hannard and F. Barthelat, Science, 2019, 364, 1260-+.
46. K. Wu, Y. Song, X. Zhang, S. Zhang, Z. Zheng, X. Gong, L. He, H. B. Yao and Y. Ni, Adv. Sci., 2022, 9.